Sequential Two (Blue) Photon Absorption by NO_2 in the Presence of H_2 as a Source of OH in Pulsed Photolysis Kinetic Studies: Rate Constants for Reaction of OH with CH_3NH_2, $(CH_3)_2NH$, $(CH_3)_3N$, and $C_2H_5NH_2$ at 295 K

S. A. Carl[†] and J. N. Crowley*

Division of Atmospheric Chemistry, Max-Planck-Institut für Chemie, Postfach 3060, D-55020 Mainz, Germany

Received: May 11, 1998; In Final Form: August 3, 1998

The use of the sequential two-photon dissociation of NO_2 (420−450 nm) in the presence of H_2 as a novel source of OH in kinetic studies has been assessed. Two-photon absorption by NO_2 at these wavelengths leads to both $O(^1D)$ and $O(^3P)$ production ((40% and 60%, respectively); the $O(^1D)$ is rapidly converted to OH in the presence of $\approx 1 \times 10^{16}$ cm^{-3} H_2 [$O(^1D) + H_2 \rightarrow OH + H$]. The H atom reacts with NO_2 to generate a further OH radical ($H + NO_2 \rightarrow OH + NO$). Laser fluences of ≈20−40 mJ cm^{-2} were used to generate between 2×10^{11} and 1×10^{12} cm^{-3} OH from an initial NO_2 concentration of $(5-13) \times 10^{14}$ cm^{-3}. OH [and $O(^3P)$] were detected by resonance fluorescence. Rate constants for the reactions of some aliphatic amines with the OH radical have been obtained at 295 K. The results obtained (in cm^3 s^{-1}) are $k(OH + CH_3NH_2) = (1.73 \pm 0.11) \times 10^{-11}$, $k(OH + (CH_3)_2NH) = (6.49 \pm 0.64) \times 10^{-11}$, $k[OH + (CH_3)_3N] = (3.58 \pm 0.22) \times 10^{-11}$, and $k(OH + C_2H_5NH_2) = (2.38^{+0.5}_{-0.15}) \times 10^{-11}$. Data for $(CH_3)_2NH$ were also obtained using the 193 nm photolysis of N_2O/CH_4 as the $O(^1D)$ source; the rate constant above is the average value obtained using both methods. The error limits include both statistical (2σ) and systematic errors.

1. Introduction

The experimental technique of flash photolysis combined with fast-response optical detection methods such as fluorescence and absorption is a versatile and powerful tool for kinetic studies of homogeneous gas-phase reactions.[1,2] Experiments are usually designed so that the generation of one of the reactants, usually a radical, takes place on a much shorter time scale that its subsequent reaction with an excess concentration of a second reactant. High-intensity, short-duration pulses of light from either flash lamps (broad band, flash duration typically >10 μs) or lasers (small bandwidths of usually <1 cm^{-1} and pulse duration typically <100 ns) are common means to generate radicals from suitable precursors. The short pulse duration, collimated and monochromatic output, and greatly increased availability of lasers over the last 20 years has made them the preferred source of light for most applications.

The laser frequency must generally coincide with an excited-state energy level of the precursor that leads to dissociation. For small molecules this often means that a UV photon is required, which explains the popularity of rare-gas excimer lasers (193, 222, 248, 308, or 351 nm) and Nd−YAG lasers (266 and 355 nm, 4ω and 3ω, respectively) as photon sources in this type of experiment.

One of the most extensively studied reactive species is the OH radical. Its important role as an oxidizing agent in both atmospheric and combustion processes has led to the assimilation of a large body of kinetic data for its reactions with both radical and stable species. A great deal of the data on OH reactions with stable molecules has been obtained by using the flash photolysis method. The commonly used OH source reactions are as follows:

$$HNO_3 + h\nu\ (193, 248, 266\ \text{nm}) \rightarrow OH + NO_2 \quad (1)$$

$$H_2O_2 + h\nu\ (193, 248, 266\ \text{nm}) \rightarrow 2OH \quad (2)$$

$$HONO + h\nu\ (351, 355\ \text{nm}) \rightarrow OH + NO \quad (3)$$

$$O_3 + h\nu\ (248\ \text{nm}) + H_2O \rightarrow 2OH + O_2 \quad (4)$$

$$N_2O + h\nu\ (193\ \text{nm}) + H_2O \rightarrow 2OH + N_2 \quad (5)$$

In reactions 1−3 the OH radical is generated directly, whereas N_2O and O_3 photolysis (reactions 4 and 5) first generates $O(^1D)$, which is converted on a very short time scale to OH in the presence of water vapor. The choice of precursor system is constrained by a number of factors. Ideally, the precursors should meet the following criteria: (a) The precursor should not react with the excess reactant. (b) The dissociative photon should not be absorbed by the excess reactant to generate unwanted radical species or excited states. (c) The precursor should not react (rapidly) with OH. Rate constants[3] (in cm^3 s^{-1}) for OH reaction at 20 Torr and 298 K are 1.1×10^{-13} (HNO_3), 1.7×10^{-12} (H_2O_2), 4.5×10^{-12} (HONO), 6.8×10^{-14}(O_3), and $<7 \times 10^{-19}$ (N_2O). (d) Highly stable flows of the precursor should be maintained over several hours typically needed to determine a rate constant. This is especially important if criterion c is not fulfilled. (e) The precursor molecules should be relatively easily synthesized and purified (or purchased).

Problems associated with mixing the precursors with the excess reactant are often encountered. The HNO_3, H_2O_2, and HONO precursors are relatively reactive and can react either in the gas phase or on surfaces with other species. One striking

[†] Present address: Department of Chemistry, University of Leuven, Celestijnenlaan 200F, B-3001 Leuven, Belgium.

S1089-5639(98)02193-8 CCC: $15.00
Published on Web 09/25/1998

example is the reaction of all three of these acidic gases with basic, aliphatic amines, which is the subject of the present study.

In the following we present a novel way of generating OH; the sequential two-photon dissociation of NO_2 in the presence of H_2, and indicate under which circumstances it provides a useful extension to the above list. It will be shown in this paper and elsewhere[4] that this OH source fulfills criteria b, d, and e particularly well, and criterion a reasonably well, but has shortcomings with respect to criterion c, and similar to reactions 4 and 5, it is not suitable for kinetic studies of OH in high pressures of N_2 or O_2 bath gas.

The aliphatic amines, especially methylamine (CH_3NH_2), dimethylamine [$(CH_3)_2NH$], and trimethylamine [$(CH_3)_3N$], have received some attention[5] in the context of atmospheric and environmental sciences due to their potential role as precursors of HCN and particularly N_2O, which is both an important greenhouse gas[6] and the main source of stratospheric NOx.[7,8] The products of the degradation of $(CH_3)_2NH$ can also lead to the production of carcinogenic nitrosamines in the polluted environment.[9]

In contrast to ammonia (NH_3), alkylamines react rapidly with the major initiator of trace gas oxidation in the troposphere, the OH radical, and their atmospheric lifetimes are determined by the OH concentration and the rate constant for reaction with OH. To date, the kinetics of the reaction between OH and alkylamines have been the subject of a single study in each case.[10,11] The paucity of data may to some extent be due to experimental problems associated with mixing the amines with suitable OH precursors, which, for photolytic sources, are often acidic gases that form aerosols in the presence of the basic amines. We have reinvestigated the room-temperature kinetics of some OH + amine reactions using a novel two-photon OH source that overcomes these problems.

2. Experimental Section

2.1. General Setup. The laser photolysis/OH resonance fluorescence experimental setup has been described in detail in recent publications.[12,13] Pulsed (5−6 ns) radiation between 432 and 445 nm was provided by a 355 nm (Nd−YAG, 3ω) pumped dye laser operating at 10 Hz with coumarin 120 dye. The laser emission was expanded to a collimated beam of about 4 mm diameter and passed through two irises before being directed into the photolysis cell. Pulse energies were monitored with a joule meter placed behind the exit Brewster window of the cell. OH radicals were excited by a microwave-powered discharge lamp (H_2O/He mixture at 3 Torr) and their fluorescence was detected at right angles to both the axis of propagation of the laser beam and the microwave lamp by a photomultiplier (EMI 9899QB) operating in photon counting mode, which was screened by a 309 ± 5 nm interference filter. Between 500 and 4000 decay profiles were averaged at 10 Hz to improve signal-to-noise ratios. $O(^3P)$ atoms were also detected by resonance fluorescence. In this case a single MgF_2 lens imaged the resonantly scattered light ($\lambda \approx 130$ nm) from $O(^3P)$ onto a photomultiplier with a CsI photocathode (Hamamatsu 1459). The microwave lamp operated at 1 Torr of ultrahigh purity helium, and the emission passed through a 2 mm thick CaF_2 window that blocked Lyman-α radiation.

During kinetic experiments, the concentrations of both NO_2 and the amines were determined by optical absorption in a separate cell with either 132 or 975 cm optical path length, which was linked serially in flow prior to the photolysis cell. The wavelength-dependent extinction of light from a D_2 or halogen lamp was measured with a diode array camera coupled to a monochromator equipped with a grating blazed at 200 or 500 nm with 600 lines/mm. This resulted in a spectral window of 82 nm width with a effective resolution of about 0.3 nm. The optical absorption and photolysis cells were connected with either Teflon or glass piping, pressures in both were measured with capacitance manometers, and flow rates were controlled by calibrated mass-flow controllers. For determination of the absorption cross-sections of the amines, a separate cell of volume ≈130 cm^3 and optical path length of 10 cm was used. The 10 cm cell was evacuated by a turbomolecular pump to better than 1×10^{-3} Torr. A 10 Torr capacitance manometer was used to monitor the pressure of the amines.

2.2. Characterization of the OH Generation Scheme. OH was generated in the following scheme:

$$NO_2 + h\nu\ (410-450\ nm) \rightarrow NO_2^* \quad (6)$$

$$NO_2^* + h\nu\ (410-450\ nm) \rightarrow NO_2^{**} \quad (7)$$

$$NO_2^{**} \rightarrow NO + O(^1D) \quad (8a)$$

$$O(^1D) + H_2 \rightarrow OH + H \quad (9)$$

$$H + NO_2 \rightarrow OH + NO \quad (10)$$

The confirmation that sequential two-photon absorption by NO_2 (420−450 nm) is responsible for the formation of $O(^1D)$ (and thus OH) was obtained in experiments where both the photolysis wavelength and laser fluence were varied when NO_2/Ar/H_2O, NO_2/Ar/H_2, or NO_2/Ar/CH_4 mixtures were photolyzed.[12] The intensity of the OH signal closely followed the structured absorption of NO_2 and displayed a quadratic dependence on laser fluence. The observation of OH is thus indirect evidence for $O(^1D)$ formation.

In this work we have further characterized the sequential, two-photon dissociation of NO_2 by carrying out experiments in which N_2 replaced the H-atom donor (H_2, H_2O, or CH_4) and in which $O(^3P)$ atoms were detected. The concentration of N_2 was 6 Torr, in a total pressure of 20 Torr (mainly Ar).

$$O(^1D) + N_2 \rightarrow O(^3P) + N_2 \quad (11)$$

$$O(^3P) + NO_2 \rightarrow NO + O_2 \quad (12)$$

$k_{11} = 2.6 \times 10^{-11}$ cm^3 s^{-1},[3] so that $O(^3P)$ generation is complete within ≈0.2 μs.

After correction for a small background signal due to stray light from the resonance lamp, the measured fluorescence decays of $O(^3P)$ were found to be exponential (Figure 1) and dependent on the concentration of NO_2 present. The NO_2 concentration was determined by fitting the optical absorption between 328 and 409 nm to a reference spectrum.[14]

For pseudo-first-order kinetics ($[NO_2] \gg [O(^3P)]$), the decay of $O(^3P)$ is described by

$$[O(^3P)]_t = [O(^3P)]_0 \exp\{-(k_{12}[NO_2] + c)t\} \quad (i)$$

where $k_{12}[NO_2]$ is defined as the pseudo-first-order rate constant (k_{1st}).

A plot of k_{1st} versus $[NO_2]$ (inset in Figure 1) should thus give the bimolecular rate constant for the reaction between $O(^3P)$ and NO_2. The slope yields $k_{12} = (1.03 \pm 0.04) \times 10^{-11}$ cm^3 s^{-1}, in good agreement with the 298 K recommended value of $(9.7 \pm 1) \times 10^{-12}$ cm^3 s^{-1}.[3] This provides confirmation that $O(^3P)$ is generated and detected in these experiments. In

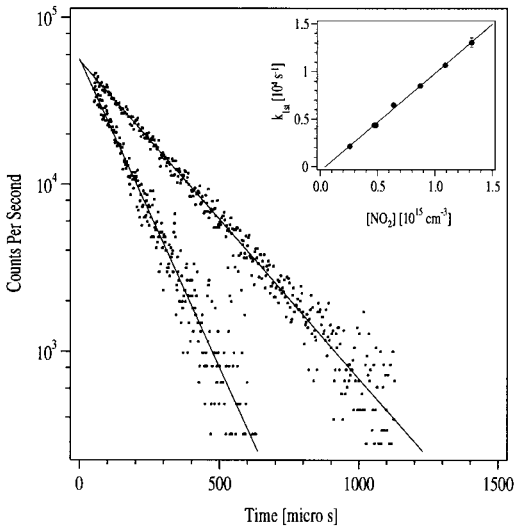

Figure 1. Decays of $O(^3P)$ in the presence of an excess concentration of NO_2. $O(^3P)$ was formed both directly in the two-photon dissociation of NO_2 at 439.4 nm and following quenching of $O(^1D)$ by N_2. The inset shows a plot of pseudo-first-order decay rate of $O(^3P)$ (k_{1st}) versus concentration of NO_2. The slope yields a 295 K rate constant for $O(^3P)$ + NO_2 of $(1.03 \pm 0.04) \times 10^{-12}$ cm^3 s^{-1} (2σ errors).

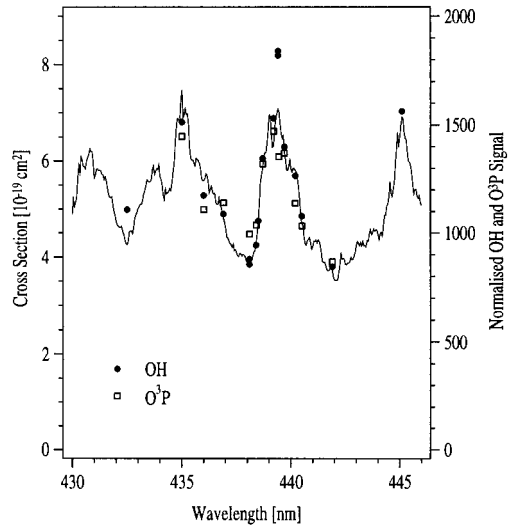

Figure 2. Dependence of OH signal (●, right *y*-axis) and $O(^3P)$ signal (□, right *y*-axis) on the photolysis wavelength, and the absorption spectrum of NO_2 (—, left *y*-axis). The experimental conditions were $[NO_2]_0 = 5 \times 10^{14}$ cm^{-3}, $[H_2] = \approx 1 \times 10^{16}$ cm^{-3}, and Ar ≈ 20 Torr. The data have been normalized to the laser fluence squared.

addition, the wavelength dependence of the $O(^3P)$ initial signal was determined between 435 and 442 nm. This variation with wavelength is shown in Figure 2 (□) along with our previously published data for OH. In both cases, normalization of the $O(^3P)$ or OH signal strength to the square of the laser fluence results in a very good correlation with the features of the NO_2 absorption spectrum, confirming that the first step in the formation of $O(^3P)$ or OH is nondissociative absorption of a photon by NO_2 to form NO_2*.

Two further sets of experiments to characterize the two-photon photochemistry were carried out by replacing N_2 with various amounts of H_2 and detecting either OH or $O(^3P)$. A plot of $O(^3P)$ and OH signal intensity versus concentration of added H_2 is given in Figure 3. Although the data were obtained in separate experiments, the flows, pressure, and $[NO_2]_0$ were kept the same. As $[H_2]$ is increased, the $O(^3P)$ signal is reduced as $O(^1D)$ is scavenged and OH is formed. The $O(^3P)$ signal

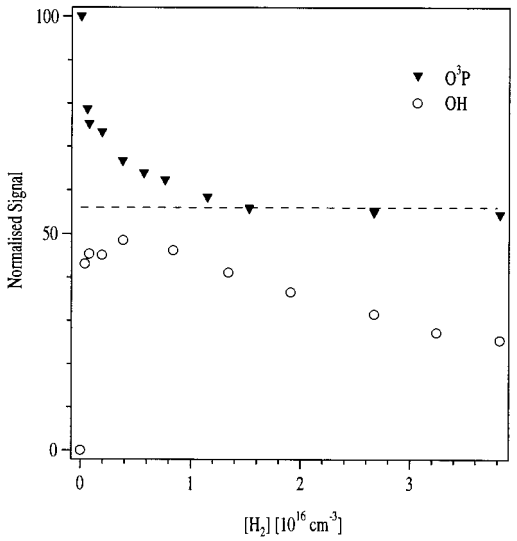

Figure 3. Initial $O(^3P)$ (▼) and OH (○) signals in the presence of various amounts of H_2. Experimental conditions were $NO_2 = 4.9 \times 10^{14}$ cm^{-3}, Ar = 20 Torr, $\lambda_{photolysis} = 439.4$ nm.

does not, however, go to zero even at high H_2. This is rationalized in terms of a further dissociation channel for NO_2**:

$$NO_2^{**} \rightarrow O(^3P) + NO \qquad (8b)$$

Our results show that ≈50−60% of the $O(^3P)$ signal is due to primary generation via reaction 8b and thus only 40−50% is due to formation and quenching of $O(^1D)$. This is in good agreement with the work of Uselmann and Lee,[15] who determined a 40% branching to $O(^1D)$ formation in the one-photon dissociation of NO_2 from its 2 $^2B_2$ state, which is accessed by radiation of wavelengths close to 220 nm. This observation also supports our prior conclusion that the NO_2** state may be identified as the 2 $^2B_2$ state. The falloff in OH signal as the H_2 concentration is increased beyond $\approx 1 \times 10^{16}$ cm^{-3} is due to quenching of the OH ($^2\Sigma^+$) fluorescence by H_2. In summary, the first photon populates the long-lived NO_2 ($^2B_1/^2B_2$) states ($\tau \approx 50$ μs), the second photon results in population of the dissociative 2 $^2B_2$ state, which yields $O(^3P)$ (≈60%) and $O(^1D)$ (≈40%). Clearly, the two-photon dissociation of NO_2 in the presence of H_2 to make OH is not efficient if N_2 is used as the bath gas, a drawback that is shared by reactions 4 and 5 when used as OH sources. The experiments reported here were therefore conducted in Ar, which quenches $O(^1D)$ inefficiently.[16]

For the study of OH reactions, separate flows of H_2, NO_2 (5% in Ar), and Ar were directed into the photolysis cell via calibrated mass-flow controllers. The fact that each of these gases can be purchased premixed in Ar (or any buffer gas) or pure, stored without decomposition, and passed through commercial mass-flow controllers represents one of the advantages of this OH source when compared to the HNO_3 and especially the O_3, H_2O_2, and HONO precursors.

The time for generation of OH depends on the concentrations of NO_2. For example, for $[NO_2]_0 = 5 \times 10^{14}$ cm^{-3} and $[H_2] = 2 \times 10^{16}$ cm^{-3}, the half-life for reaction of $O(^1D)$ with H_2 under these conditions is about 0.5 μs, the H atom formed is converted to OH in ≈60 μs (three half-lives). Replacing the H_2 with H_2O as $O(^1D)$ scavenger reduces the OH generation period to less than 1 μs if $[H_2O] = 1 \times 10^{16}$ cm^{-3}. In our resonance−fluorescence detection scheme, this has, however, the unwanted effect of reducing the sensitivity to OH, due to very efficient quenching of the fluorescing OH ($^2\Sigma^+$) state by H_2O.

The size of the OH signal depends linearly on the NO_2 concentration and quadratically on the laser fluence. Typically, laser fluences of ≈20−40 mJ cm^{-2} were used to generate between ≈2 × 10^{11} and 1 × 10^{12} OH cm^{-3} from 5 × 10^{14} cm^{-3} NO_2.

With $[NO_2] = 5 \times 10^{14}$ cm^{-3} and at a total pressure of 20 Torr Ar, the loss rate of OH due to reaction 13 is about 400 s^{-1} before the excess reactant is added.

$$OH + NO_2 + M \rightarrow HNO_3 + M \qquad (13)$$

The rate constant for reaction 13 is 0.7 × 10^{-12} cm^3 s^{-1} at 295 K and 20 Torr total pressure Ar. This increases to 2.1 × 10^{-12} cm^3 s^{-1} at 100 Torr, implying a loss rate of about 1100 s^{-1} for OH due to reaction with NO_2 alone. At 250 K, the 20 and 100 Torr rate constants are 1.5 × 10^{-12} and 4.2 × 10^{-12} cm^3 s^{-1}, respectively. (Rate constants are from ref 3 and have been corrected by a factor of ≈0.6 for the reduced third-body efficiency of Ar compared to air or N_2.[17]) The rapid loss of OH via reaction 13 at high pressures violates condition c as outlined in the Introduction and can represent an important drawback of this OH source, which may even rule it out for high-pressure/low-temperature applications.

The OH ($X^2\Pi$) formed in the reaction between $O(^1D)$ and H_2 is vibrationally excited, with $v = 1$, $v = 2$, and $v = 3$ vibrational levels roughly equally populated, and only about 35% of the OH formed is OH ($X^2\Pi$, $v = 0$).[18] Similarly, ≈70% of the OH from the reaction of H with NO_2 is vibrationally hot with $v = 1$ produced at 1.3 times the rate of $v = 0$, and some excitation of $v = 2$ (and to a small extent $v = 3$) also observed.[19] The vibrationally excited $v = 2$ state is only slowly quenched by Ar, He, N_2, or H_2 with an upper limit[20] to the quenching rate constant of 1 × 10^{-14} cm^3 s^{-1}, though the $v = 1$ state is rapidly deactivated by collision with both NO ($k = 3.8 \times 10^{-11}$ cm^3 s^{-1}) and NO_2 ($k = 4.8 \times 10^{-11}$ cm^3 s^{-1})[21]. This implies that in our experiments with $[NO_2] > 5 \times 10^{14}$ cm^{-3}, hot OH (at least $v = 1$) would be quenched in <40 μs. Also, neither in experiments carried out on OH + NO_2 in this laboratory[22] with the NO_2 + 2 $h\nu$ source of OH nor in low-pressure discharge-flow studies of OH + NO_2 in either He or Ar was any evidence obtained for a changed reactivity of OH due to vibrational excitation,[23−27] which would manifest itself as curvature in the plots of the low-pressure bimolecular rate constant versus pressure of bath gas. We conclude therefore that vibrational excitation of OH is unlikely to be a problem in the present study.

2.3. Kinetics of OH + Amines. The use of the above scheme for OH generation overcomes difficulties associated with mixing the traditional photolytic OH sources HNO_3, H_2O_2, and HONO with the amines. The mixing of these acidic gases with the strongly basic amines results in aerosol formation even at low partial pressures as evidenced by our own spectroscopic observations of light scattering (using HNO_3 and H_2O_2) and literature observations[28,29] with HONO. We tested the applicability of mixing Ar/NO_2/H_2/amine flows by optically monitoring the amine concentration (≈2 × 10^{14} cm^{-3} diluted in Ar) both prior to and after adding the Ar/NO_2/H_2 flow (with $[NO_2] = 5 \times 10^{14}$ cm^{-3}). No measurable change in [amine] was observed, showing that no significant reaction took place within the residence time of both gases in the apparatus (about 20 s), in agreement with the conclusions of Hanst et al.[28] that NO and NO_2 react only slowly with $(CH_3)_2NH$ in comparison to HONO. There was also no measurable extinction of light from a D_2 lamp that could be assigned to aerosol formation. Despite this, at the point of mixing of the Ar/NO_2/H_2 flow with the Ar/amine flow, some white deposit built up over the time scale of a few hours on the glass surface. Aerosol formation has also been observed when high concentrations (20 Torr) of NO (and NO_2) are mixed with similar amounts of $(CH_3)_2NH$ in a reaction to make nitrosamine.[28]

For studying the kinetics of the reaction of OH with CH_3NH_2, $C_2H_5NH_2$, $(CH_3)_2NH$, and $(CH_3)_3N$, the H_2 concentration was set at about 1 × 10^{16} cm^{-3} compared to typical amine concentrations of between 1.5 × 10^{13} and 4 × 10^{14} cm^{-3}. This ensures that the fate of $O(^1D)$ is dominated by reaction 9. NO_2 concentrations were held at about (5−13) × 10^{14} cm^{-3}, resulting in H atom conversion to OH (reaction 3) in ≈60 μs (three half-lives for H). This OH generation period is very short compared to the time scales of the OH decay and compared to the period following the laser flash in which stray light and electronic interference prevented measurement (≈200 μs). Generally the photolysis wavelength was 439.4 nm, which is close to a peak of a NO_2 absorption feature. As the amines also possess strong absorption spectra in the region between 190 and 250 nm, the use of dissociative UV radiation (i.e., at 193 nm) could potentially complicate the kinetics by formation of reactive and electronically excited radicals.[30,31] However, in an additional set of experiments, the 193 nm photolysis of N_2O followed by reaction 14 was used as an alternative OH source:

$$N_2O + h\nu\ (193\ nm) \rightarrow N_2 + O(^1D) \qquad (5)$$

$$O(^1D) + CH_4 \rightarrow CH_3 + OH \qquad (14)$$

Radiation (193 nm, 20 ns pulse duration) was provided by an excimer laser with ArF gas mixture. Diluted mixtures of NO_2/Ar or N_2O/Ar (between 0.5% and 1%) and amine/Ar (between 0.1% and 0.5%) were passed through calibrated mass-flow controllers and premixed with flows of H_2 (or CH_4) and Ar before entering the optical absorption cell. The concentration of amine was then determined by deconvoluting the measured optical density ($200 < \lambda < 280$ nm) into the NO_2 and amine components. For this, absorption spectra of NO_2 and amine were used that had been measured at the same resolution using the same diode array/monochromator.

The gases CH_3NH_2 (Linde, 99%), $C_2H_5NH_2$ (Linde, 99.7%), $(CH_3)_2NH_2$ (Linde, 99%), $(CH_3)_3N$ (Linde, 99%), Ar (Linde, 99.999%), H_2 (Linde, 99.999%), NO_2 (purchased as N_2O_4, Merck, 99.5%), and N_2O (Hoechst, 99.5%) were used without further purification.

3. Results

3.1. UV Absorption Spectra. Figures 4 and 5 display the absorption cross sections of CH_3NH_2, $C_2H_5NH_2$, $(CH_3)_2NH$, and $(CH_3)_3N$ between 196 and 250 nm at ≈0.3 nm resolution. Spectra obtained at various pressures between 0.1 and 2 Torr displayed Beer−Lambert linearity, and the final spectrum is the average of at least four measurements at different pressures. All of the spectra display a continuous absorption with a variable amount of vibronic structure and are consistent in both shape and intensity with the measurements of Tannenbaum et al.[32] Although a detailed comparison of the spectra was not possible as the Tannenbaum et al. cross sections could only be read from a figure given in their paper, the cross-sections agreed within 10%. As our cross sections were measured by diode-array spectroscopy and displayed Beer−Lambert linearity throughout the wavelength range covered, we estimate that errors are due only to purity and pressure measurement and should not exceed 5%.

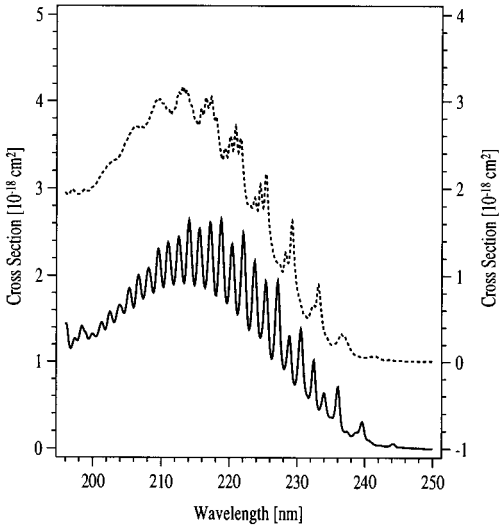

Figure 4. UV absorption spectra of CH_3NH_2 (—, left *y*-axis), and $C_2H_5NH_2$ (---, right *y*-axis).

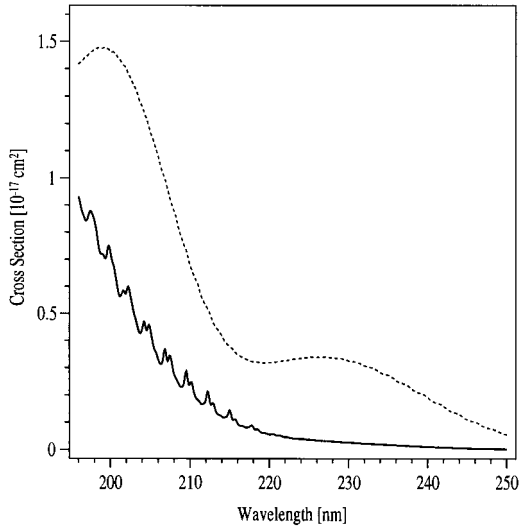

Figure 5. UV absorption spectra of $(CH_3)_2NH$ (—), and $(CH_3)_3N$ (---).

3.2. OH Kinetics. The reactions were carried out under pseudo-first-order conditions ([amine] ≫ [OH]), and the OH decay is expected to be exponential and described by

$$[OH]_t = [OH]_0 \exp\{-(k_{bi}[\text{amine}] + k_{NO_2}[NO_2] + d)t\} \quad \text{(ii)}$$

where $[OH]_t$ is the OH concentration at time t after the laser pulse, k_{bi} is the bimolecular rate constant for the reaction of OH with the amine, k_{NO_2} is the rate constant for reaction of OH with NO_2, and d is the rate constant for diffusion out of the reaction volume. The first-order decay rate constant, k_{1st}, was obtained by the nonlinear least-squares fitting of the decays and is related to the desired rate constant (k_{bi}) by

$$k_{1st} = k_{bi}[\text{amine}] + k_{NO_2}[NO_2] + d \quad \text{(iii)}$$

To determine k_{bi}, the amine concentration must be accurately known and was obtained in each case by optical absorption spectroscopy (see above).

For each amine, experiments were carried out in which the laser fluence was varied by up to a factor of 2, resulting in a factor of 4 change in $[OH]_0$ owing to the quadratic dependence on energy of the two-photon process. In addition, the laser repetition rate was decreased to 2 Hz rather than the normal 10 Hz. Neither of these changes had any discernible influence on the measured OH decay rates. Under the given conditions of flow rate and total pressure in a typical experiment, there was a small pressure gradient between the optical absorption cell and the photolysis cell of about 1 Torr when White optics were used and about 0.1 Torr when single-pass measurements were carried out. The optically determined amine concentration was thus corrected downward (by a maximum of 5%) to take this into account. Variation of the pressure difference in the two cells of up to 20 Torr (40 Torr in the optical absorption cell and 20 Torr in the photolysis cell) resulted in no change in the OH decay rate for a given [amine].

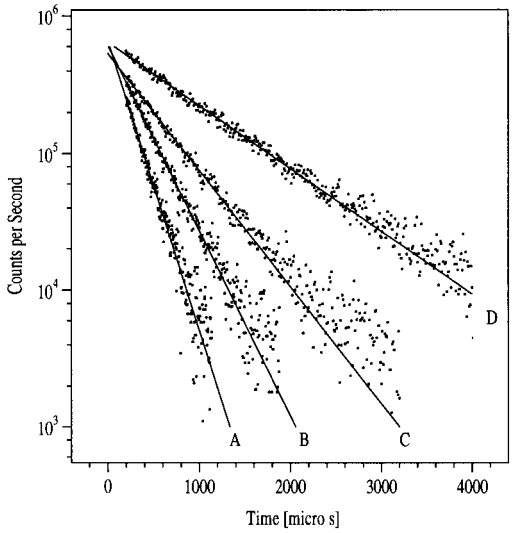

Figure 6. Pseudo-first-order decays of OH in the presence of various excess concentrations of CH_3NH_2. $[CH_3NH_2] = 2.20 \times 10^{14}$, 1.21×10^{14}, and 5.72×10^{13} cm^{-3} for curves A, B, and C, respectively. Curve D was obtained in the absence of CH_3NH_2; the decay of OH is due mainly to reaction with NO_2.

As the polar amines have a high affinity for surfaces, some conditioning of the flow controller, glass mixing lines, quartz cell for absorption measurements, and Teflon-coated photolysis cell was necessary before stable concentrations were obtained. Under typical flow conditions and an amine concentration of about 1×10^{14} cm^{-3}, about 20 min was necessary at the beginning of each day's experiments to condition the whole system. A stable concentration was characterized by a time-independent optical absorption due to the amine and a constant OH decay rate for a given stable flow of the gas mixture. Once this conditioning period was over, changes in the partial flow rate of the amine resulted in rapid changes in optical density (ca. 1 min to establish a stable concentration at the new flow rate). Generally 10 min was allowed to lapse between establishing the new flow rate and measuring the OH decay rate. Measurements were made with amine flow rates varied in both increasing and decreasing directions to test for hysteresis effects, which were not observed.

3.2.1. CH_3NH_2. Typical OH decays ($[OH]_0 \approx 5 \times 10^{11}$ cm^{-3}) in the presence of different excess concentrations of CH_3NH_2 are displayed in Figure 6 and are seen to be exponential over at least three half-lives. The decay in the absence of CH_3NH_2 (profile D) is due mainly to reaction with NO_2.

For each OH decay, an optical measurement was carried out to determine the CH_3NH_2 concentration. Figure 7 shows the measured optical density of a flowing $Ar/NO_2/CH_3NH_2/H_2$ mixture and the deconvoluted contributions from NO_2 and CH_3NH_2. The absolute cross sections of CH_3NH_2 shown in Figure 4 enabled its concentration to be accurately determined, with

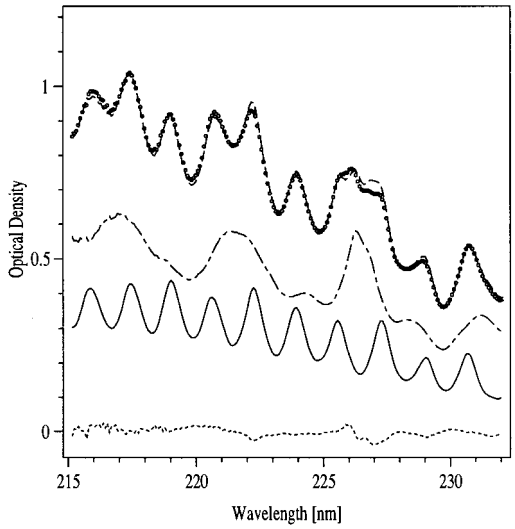

Figure 7. Measured (○) and fitted (− − −) optical densities and deconvoluted absorption due to NO_2 (− - −) and CH_3NH_2 (—). The residual absorption (---) is the difference between the total measured optical density and the sum of the NO_2 and CH_3NH_2 absorptions. For this particular measurement, $[CH_3NH_2] = 1.55 \times 10^{14}$ cm^{-3} and $[NO_2] = 1.30 \times 10^{15}$ cm^{-3}.

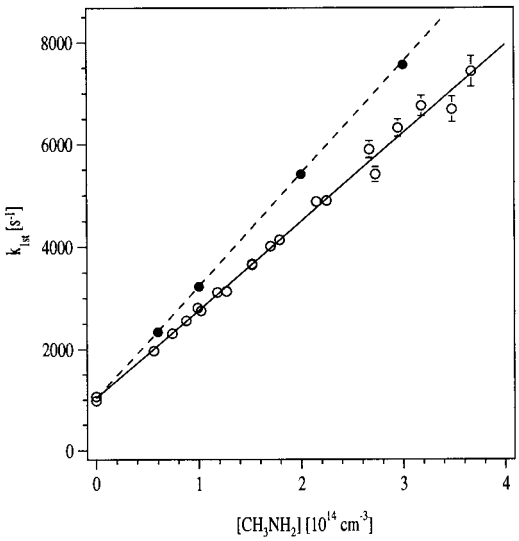

Figure 8. Plot of pseudo-first-order rate (k_{1st}) against concentration of CH_3NH_2. (− − −) Expected rates based on the OH rate constant of Atkinson et al.;[10,11] (●) simulated rates including the effect of OH reformation via the reaction of O(^{3}P) with the amine. (○) Experimental data obtained in this work with least-squares fit (—). The rate constant obtained from the slope of the fit is $(1.73 \pm 0.06) \times 10^{-11}$ cm^3 s^{-1} (2σ errors).

statistical errors as low as 1.5% for a 1.5×10^{14} cm^{-3} sample. The plot of pseudo-first-order decay rate (k_{1st}) versus [CH_3NH_2] enables the rate constant to be obtained (eq iii), as shown in Figure 8. The nonlinear least-squares fit to the data in Figure 8 yields a 295 K rate constant of $k(OH + CH_3NH_2) = (1.73 \pm 0.06) \times 10^{-11}$ cm^3 s^{-1} (error limits are 2σ).

3.2.2. $(CH_3)_2NH$. OH decays of between 1600 and 6000 s^{-1} were measured in excess concentrations of $(CH_3)_2NH$ ranging from 1.3×10^{13} to 0.7×10^{14} cm^{-3}. The absolute concentration of $(CH_3)_2NH$ was obtained from the cross sections displayed in Figure 5; however, due to the comparative lack of vibronic structure, the spectral deconvolution procedure is less accurate for $(CH_3)_2NH$ than for CH_3NH_2. The errors associated with the concentration determination may therefore approach 10% at low concentrations, though they are low (3%) at higher

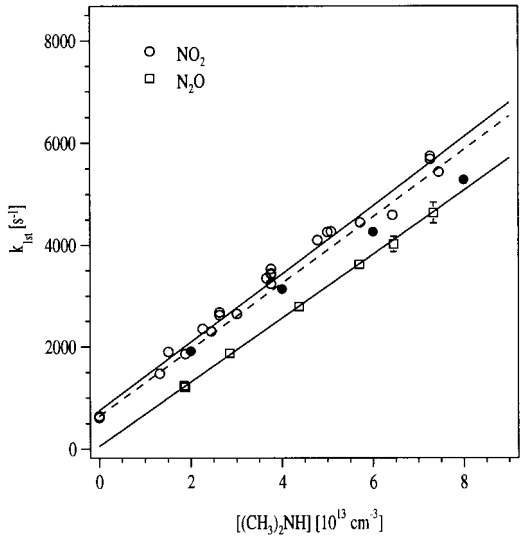

Figure 9. Plot of pseudo-first-order rate (k_{1st}) against concentration of $(CH_3)_2NH$. (− − −) Expected rates based on the OH rate constant of Atkinson et al.;[10,11] (●) simulated rates including the effect of OH reformation via the reaction of O(^{3}P) with the amine. (○) Experimental data obtained in this work with least-squares fit (—). The rate constant obtained from the slope is $(6.70 \pm 0.34) \times 10^{-11}$ cm^3 s^{-1} (2σ errors). (□) Data obtained from the 193 nm photolysis of N_2O in the presence of CH_4 as OH source; note that these symbols have been shifted down by 400 s^{-1} for clarity. These data yield a rate constant of $(6.27 \pm 0.32) \times 10^{-11}$ cm^3 s^{-1} (2σ errors).

concentrations. The plot of OH decay rate versus $[(CH_3)_2NH]_0$ is shown in Figure 9. The slope of this plot yields a rate constant of $k[OH + (CH_3)_2NH] = (6.70 \pm 0.34) \times 10^{-11}$ cm^3 s^{-1} (error limits are 2σ).

For $(CH_3)_2NH$, additional experiments were carried out using a different OH source: the 193 nm photolysis of N_2O in the presence of CH_4 (reactions 5 and 14). N_2O does not absorb as strongly as NO_2 in the region where $(CH_3)_2NH$ absorbs (simplifying the optical deconvolution measurements), does not react with OH, and is expected to be inert with respect to reaction with $(CH_3)_2NH$. The disadvantage is that the absorption cross section for $(CH_3)_2NH_2$ is 50 times greater that that of N_2O at 193 nm and that some dissociation of $(CH_3)_2NH$ is unavoidable. Control experiments in the absence of N_2O and CH_4 showed that a relatively weak fluorescence signal was obtained following the 193 nm laser photolysis of $(CH_3)_2NH$ at the same concentrations used for the OH kinetics. This signal was present, although weaker, even when the OH excitation source was turned off, implying that our detection system was seeing emission from excited electronic states of photofragments formed from 193 nm photolysis, as has been previously reported for CH_3NH_2.[33] The half-life of the emission was greater than 100 μs under our experimental conditions, precluding assignment to the NH ($A^3\Pi$) state, which emits close to our interference filter window (309 ± 5 nm) but has a collision-free half-life of $\approx$500 ns.[31] The size of the fluorescence signal was, however, too small and its decay rate too slow to seriously affect our OH signals for the N_2O photolysis experiments.

CH_4 was used as the O(^{1}D) scavenger due to apparent nonprompt OH formation when H_2 was used, even with high H_2 flows with $[H_2] = 5 \times 10^{16}$ cm^{-3}, for which a half-life of O(^{1}D) of 200 ns can be calculated. This is presumably due to the presence of small amounts of NO_2 in the N_2O/Ar bulb, which can scavenge the H atom formed in reaction 9 and results in a slow production of OH. The concentration of NO_2 necessary to do this is $\approx 1 \times 10^{-3}[N_2O]$, which seems reasonable given the stated purity of N_2O of 99.5%.

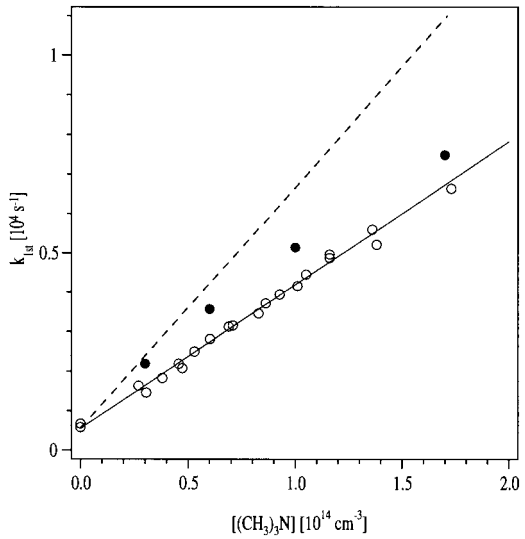

Figure 10. Plot of pseudo-first-order rate (k_{1st}) against concentration of $(CH_3)_3N$. (– – –) Expected rates based on the OH rate constant of Atkinson et al.;[10,11] (●) simulated rates including the effect of OH reformation via the reaction of $O(^3P)$ with the amine. (○) Experimental data obtained in this work with least-squares fit (—). The rate constant obtained from the slope of the fit is $(3.58 \pm 0.13) \times 10^{-11}$ cm^3 s^{-1}.

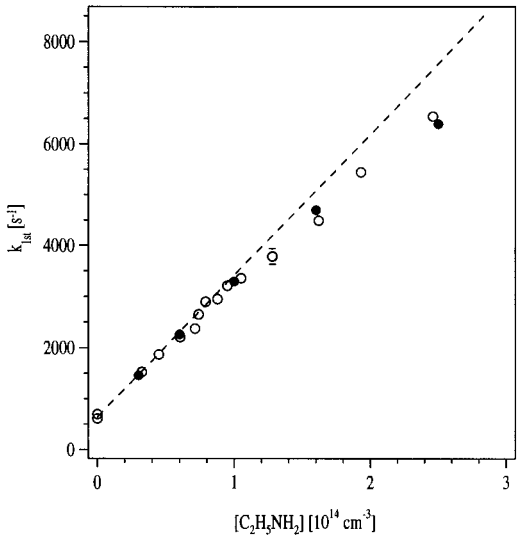

Figure 11. Plot of pseudo-first-order rate against concentration of $C_2H_5NH_2$. (– – –) Expected rates based on the OH rate constant of Atkinson et al.[10,11] (●) simulated rates including OH reformation via the reaction of $O(^3P)$ with the amine. (○) Experimental data obtained in this work.

This slow formation of OH was not observed when CH_4 replaced H_2, as CH_3 is formed instead of H. The fate of the CH_3 fragment is probably reaction with NO_2 ($k_{15} = 2.4 \times 10^{-11}$ cm^3 s^{-1}),[34] and the CH_3O product is also rapidly converted to CH_3ONO_2 ($k_{16} = 6.0 \times 10^{-12}$ cm^3 s^{-1} at 20 Torr).[3]

$$CH_3 + NO_2 \rightarrow CH_3O + NO \quad (15)$$

$$CH_3O + NO_2 \rightarrow CH_3ONO_2 \quad (16)$$

As the initial concentration of CH_3 is the same as that of OH (i.e., less than 1×10^{12} cm^{-3}), reaction with CH_3ONO_2 will not contribute to the decay of OH. Based on the measured laser fluence, and the known cross section of $(CH_3)_2NH$ at 193 nm, about 2% of the $(CH_3)_2NH$ is dissociated in the laser pulse. Even if the photofragments react with a rate constant of 1×10^{-10} with OH, this will enhance the OH decay rate by just 4%. This could be confirmed in experiments in which the laser fluence was reduced by a factor of 2, while the amine concentration was held constant. Within experimental scatter, this had no effect on the OH decay rate.

The plot of k_{1st} versus $[(CH_3)_2NH]$ derived from these experiments is also displayed in Figure 9. The slope yields a rate constant of $(6.27 \pm 0.32) \times 10^{-11}$ cm^3 s^{-1}, agreeing within the combined (statistical) error limits to that obtained using NO_2 photolysis.

3.2.3. $(CH_3)_3N$. As the UV absorption cross sections of $(CH_3)_3N$ are so high ($\sigma_{max} = 1.5 \times 10^{-17}$ cm^2 at 200 nm), the kinetic experiments with $(CH_3)_3N$ were carried out using the single-pass optical absorption setup. As the $(CH_3)_3N$ spectrum has no vibronic structure, a wide wavelength range between 200 and 260 nm was used to perform the fitting. In this case, the occurrence of two maxima in the spectrum of $(CH_3)_3N$ enable the fits to be carried out with high accuracy (±2%) despite problems associated with baseline drift over the course of a few hours. OH decays were measured in the presence of between 3.05×10^{13} and 1.73×10^{14} cm^{-3} $(CH_3)_3N$. The plot of pseudo-first-order decay rate versus $[(CH_3)_3N]$ is shown in Figure 10. The rate constant obtained is $k[OH + (CH_3)_3N] = 3.58 \pm 0.13$ cm^3 s^{-1} at 295 K (error limits are 2σ).

3.2.4. $C_2H_5NH_2$. Initial experiments with $C_2H_5NH_2$ were carried out with White optics and a 975 cm optical path length to determine concentrations. We found, however, that the $C_2H_5NH_2$ spectrum was heavily contaminated with that of $(CH_3)_2NH$. This is most likely due to the displacement of $(CH_3)_2NH$ from the stainless steel surface of the White optic mounts, as $(CH_3)_2NH$ experiments had been carried out prior to those with $C_2H_5NH_2$. These problems were not observed during the measurement of the UV absorption spectra of the amines and disappeared when the White optics were removed from the absorption cell and it was converted into a single-pass system ($l = 132$ cm).

OH decays were measured in excess concentrations of $C_2H_5NH_2$ between about 3.2×10^{13} and 2.5×10^{14} cm^{-3}. The plot of k_{1st} versus $[C_2H_5NH_2]$ is given in Figure 11. The rate constant obtained by fitting a straight line to the data in Figure 11 is $k(OH + C_2H_5NH_2) = (2.38 \pm 0.10) \times 10^{-11}$ cm^3 s^{-1} (error limits are 2σ). The kinetic results for all amines are summarized in Table 1.

4. Discussion

Before we compare our results to those obtained in previous studies (see below), we consider potential systematic errors introduced by the simultaneous generation of both $O(^1D)$ and $O(^3P)$ in our experiments. As already mentioned, the ratio of $O(^1D)$ to $O(^3P)$ generated in the two-photon dissociation of NO_2 close to 440 nm is 40:60. The fate of the $O(^1D)$ is determined by the relative rates of reaction with H_2 and quenching by the Ar bath gas. Using $k[O(^1D) + H_2 \rightarrow OH + H] = 1.1 \times 10^{-10}$ cm^3 s^{-1} and $k[O(^1D) + Ar \rightarrow O(^3P)] = <5 \times 10^{-13}$ cm^3 s^{-1}, $[H_2] = 1 \times 10^{16}$ cm^{-3} and 20 Torr of Ar, we calculated that 21% of the $O(^1D)$ is quenched to $O(^3P)$. This results in an upper limit to the initial $O(^3P)$/OH ratio of 2.2. The presence of $O(^3P)$ can perturb the OH kinetics either by reacting directly with OH, by depleting the amine concentration, or by generating OH via reaction with the amine. As the experiments were carried out with low conversion of NO_2 and low initial concentrations of OH and $O(^3P)$, the first two problems are insignificant. However, the reaction of $O(^3P)$ with amines has been shown, in some cases, to be rapid[35] with the following room-temperature

TABLE 1: Summary of Kinetic Results and Comparison with Literature

reactant	[amine] (cm^{-3})	no. of decays	range of k_{1st} (s^{-1})	k_{bi} (this work) ($cm^3\ s^{-1}$)	k_{bi} (refs 10 and 11) ($cm^3\ s^{-1}$)
CH_3NH_2	$5.60 \times 10^{13} - 3.67 \times 10^{14}$	19	1970−7430	$(1.73 \pm 0.11) \times 10^{-11}$	$(2.20 \pm 0.22) \times 10^{-11}$
$(CH_3)_2NH$	$1.31 \times 10^{13} - 0.73 \times 10^{14}$	22[a]	1480−5680	$(6.70 \pm 0.47) \times 10^{-11}$	$(6.54 \pm 0.66) \times 10^{-11}$
	$1.89 \times 10^{13} - 0.74 \times 10^{14}$	6[b]	1600−5040	$(6.27 \pm 0.44) \times 10^{-11}$	
				$(6.49 \pm 0.64) \times 10^{-11}$ [c]	
$(CH_3)_3N$	$3.05 \times 10^{13} - 1.73 \times 10^{14}$	19	1460−6700	$(3.58 \pm 0.22) \times 10^{-11}$	$(6.09 \pm 0.61) \times 10^{-11}$
$C_2H_5NH_2$	$3.24 \times 10^{13} - 2.46 \times 10^{14}$	14	1530−6640	$(2.38^{+0.5}_{-0.15}) \times 10^{-11}$	$(2.77 \pm 0.28) \times 10^{-11}$

[a] Using the NO_2/H_2 + 439.4 nm source of OH. [b] Using N_2O/CH_4 + 193 nm source of OH. [c] Average value from both OH sources. The error limits quoted for data from the present study include an estimated systematic error of 5% associated with amine concentration determination. For 439.4 nm experiments, the NO_2 concentration was varied between 5×10^{14} and 13×10^{14} cm^{-3}, the laser fluence (at 439.4 nm) between 20 and 40 mJ/cm^2, and the initial OH concentration between 2×10^{11} and 10×10^{11} cm^{-3}.

rate constants: $k_{17} = 5.6 \times 10^{-13}$, $k_{18} = 6.0 \times 10^{-12}$, $k_{19} = 2.2 \times 10^{-11}$, and $k_{20} = 1.3 \times 10^{-12}$ $cm^3\ s^{-1}$.

$$O(^3P) + CH_3NH_2 \rightarrow OH + \text{products} \quad (17)$$

$$O(^3P) + (CH_3)_2NH \rightarrow OH + \text{products} \quad (18)$$

$$O(^3P) + (CH_3)_3N \rightarrow OH + \text{products} \quad (19)$$

$$O(^3P) + C_2H_5NH_2 \rightarrow OH + \text{products} \quad (20)$$

To assess potential errors due to the formation of OH in reactions 17−20, numerical simulations of the reaction system were carried out for each amine.[36] The simulations were initialized with OH and $O(^3P)$ concentrations of 5.0×10^{11} and 1.1×10^{12} cm^{-3}, respectively, and with a series of initial concentrations for each amine that matched the range covered experimentally. In addition, the experimentally determined initial NO_2 concentrations were also used and were determined by spectral deconvolution of the composite NO_2 + amine absorption spectra (e.g., Figure 7). The initial NO_2 concentrations were 1.3×10^{15}, 6.2×10^{14}, 5.0×10^{14}, and 4.8×10^{14} cm^{-3} for experiments with CH_3NH_2, $(CH_3)_2NH$, $(CH_3)_3N$, and $C_2H_5NH_2$, respectively. The NO_2 concentration is important as reaction 12 partially determines the fate of the $O(^3P)$ and competes with conversion of $O(^3P)$ to OH via reaction with the amines. The reaction scheme therefore included the reactions between both OH and $O(^3P)$ with the amine and with NO_2. For initial simulations, the kinetic data of Atkinson et al. were taken. for the reactions of $O(^3P)$[35] and OH[10,11] (hereafter ATK78/9) with the amines. The rate constant for $O(^3P)$ and OH with NO_2 were taken from ref 3, and that for OH + NO_2 was corrected for bath gas efficiency. ($k_{O+NO_2} = 9.7 \times 10^{-12}$ $cm^3\ s^{-1}$ and $k_{OH+NO_2} = 7.2 \times 10^{-13}$ $cm^3\ s^{-1}$ at 295 K in 20 Torr Ar.) Note that this scheme implicitly assumes 100% yield of OH for reaction of $O(^3P)$ with each amine, that has not been proven experimentally (see later), and also uses an initial $O(^3P)$/OH ratio that is based on the upper limit to the quenching rate constant of $O(^1D)$ by Ar. Hence the simulated perturbation is also expected to be an upper limit.

The influence of reactions 17−20 on the OH decay was assessed by generating synthetic OH decays using the rate constant data of ATK78/9 decays both with and without these reactions included. The synthetic OH decay was then fitted by the same nonlinear least-squares fitting procedure as used for the real data. The slope (k_{1st}^{syn}) was then plotted against the initial amine concentration to generate a synthetic second-order plot to compare with the measured ones. All the synthetic decays of OH for reaction with all the amines were exponential at $T > 200$ μs (where our experimental data begins), or the deviation from exponential was too small to be observable in a real experiment with scatter.

For CH_3NH_2, which has the lowest $O(^3P)$ + amine rate constant, the synthetic second-order plot with reaction 17 included (●, in Figure 8) was perfectly linear and almost indistinguishable from that with reaction 17 omitted (− − −, Figure 9). The fitted (synthetic) rate constant was 2.18×10^{-11}. Thus the effect of reaction 17 is to lower the rate constant for OH + CH_3NH_2 by less than 1% (the original value of ATK78/9 was 2.20×10^{-11} $cm^3\ s^{-1}$) and may be regarded as negligible. The rate constant for reaction of $(CH_3)_2NH$ with $O(^3P)$ is rapid and the effect of reaction 18 on the OH decay may be expected to be greater. The result of the simulations for $(CH_3)_2NH$ are shown in Figure 9. The simulated second-order plot (●) clearly describes a curve, with a pronounced lowering of the rate constant at $[(CH_3)_2NH] > 4 \times 10^{13}$ cm^{-3}, an effect that is not discernible in the real experiments as any curvature would be masked by scatter. In addition, we note that the experiments that used N_2O photolysis at 193 nm as the OH source generate much less $O(^3P)$. In this case the $O(^3P)$ arose through quenching of $O(^1D)$ by Ar and was not formed directly. The initial $O(^3P)$/OH ratio is estimated as only 0.08. As the rate constant obtained with this source is in good agreement with that obtained using NO_2 + 2 $h\nu$, we conclude that the presence of $O(^3P)$ has no significant influence on the OH decay profile at $t > 200$ μs in the reaction with $(CH_3)_2NH$.

The data for $(CH_3)_3N$ and the results of the numerical simulations are summarized in Figure 10. The dashed line represents the rate constant of ATK78/9, the solid circles are the predicted effect of the regeneration of OH under our experimental conditions. The simulated data points show significant curvature, with the rate constant obtained at low $[(CH_3)_3N]$ (obtained by fitting to the first two points only) equal to 5.4×10^{-11} $cm^3\ s^{-1}$, whereas that obtained at high $[(CH_3)_3N]$ is only 3.3×10^{-11} $cm^3\ s^{-1}$. Although the effect of the regeneration of OH via reaction of $(CH_3)_3N$ with $O(^3P)$ is to lower the rate constant toward our measured values (○, Figure 11), the pronounced curvature that this reaction introduces is not reproduced in our data, which is very well fit by a straight line.

Figure 11 shows the results of the simulations for $C_2H_5NH_2$. The dashed line represents the rate constant of ATK78/9, while the solid circles are the calculated first-order rates of the simulation. The simulated rates are close to our measured values, and in this case, there is a curvature in the simulated data that appears to be reproduced by our data. We therefore prefer to quote our result for $C_2H_5NH_2$ with asymmetric error bars, as $(2.38^{+0.5}_{-0.15}) \times 10^{-11}$ $cm^3\ s^{-1}$.

In summary, for CH_3NH_2 the predicted effects of $O(^3P)$ conversion to OH were too small to be significant due to the slow rate constant of CH_3NH_2 with $O(^3P)$. For both $(CH_3)_2$-NH and $(CH_3)_3N$ the regeneration of OH was predicted to perturb our second-order plots to an extent that was not observed in our data. This might imply that the efficiency of OH

formation from the reaction of $O(^3P)$ with these amines is significantly lower that the 100% used in the simulations. This is indeed speculated upon by Atkinson and Pitts,[35] who suggest that $O(^3P)$ may add to the amine to form N-oximes, which are stable with respect to $O(^3P)$ and the respective amine. For $(CH_3)_3N$ the N-oxime is a stable species; in the case of CH_3NH_2, $C_2H_5NH_2$, and $(CH_3)_2NH$ the N-oxime may subsequently isomerize to the more stable hydroxylamine. Some evidence for this is provided by the high room-temperature rate constant and negative temperature dependence observed for $O(^3P) + (CH_3)_3N$, which is strongly indicative of formation of an energized association complex, rather than a H-atom abstraction. As mentioned by Atkinson and Pitts, similar behavior has been observed for $O(^3P)$ reaction with sulfur compounds CH_3SH, C_2H_5SH, and CH_3SCH_3, which proceed by addition. Indeed, the lack of curvature in our data for $(CH_3)_2NH$ and especially $(CH_3)_3N$ seems to indicate that an OH-forming, H-abstraction reaction between $O(^3P)$ and these amines is not the major reaction pathway. Only for $C_2H_5NH_2$ do our data reveal the curvature expected, and we conclude that our rate constant for OH with $C_2H_5NH_2$ is a lower limit. Our modeling suggests that the real value is close to the rate constant of 2.77×10^{-11} cm^3 s^{-1} as measured by ATK78/9.

To properly assess the potential influence of $O(^3P)$ we carried out a separate set of experiments in which the generation of OH resulting from reaction of $O(^3P)$ with $(CH_3)_3N$ was examined. In these experiments the 351 nm photolysis of NO_2 (XeF excimer laser) replaced the 439.4 nm photolysis and served to generate $O(^3P)$ only.[3] With a 351 nm laser fluence of 4.6 mJ cm^{-2}, (measured with a calibrated joule meter) either 2.8×10^{12} or 1.5×10^{12} cm^{-3} $O(^3P)$ was generated in the photolysis of 7.8×10^{14} or 4.0×10^{14} cm^{-3} NO_2, respectively. Varying amounts of $(CH_3)_3N$ were added to the flowing mixture (flow conditions and pressure, etc., were kept as usual) in order to test for the formation of OH. The absolute $(CH_3)_3N$ and NO_2 concentrations were determined by optical absorption as already described. Figure 12 shows the result of one experiment (experimental conditions in the figure caption). OH is clearly formed, and as expected, both generation and loss processes are evident in its time profile. The OH signal was put on an absolute basis by conducting experiments under unchanged conditions, except that NO_2 was replaced by HNO_3 (which was also determined optically) and the XeF excimer gas was replaced by KrF to give a 248 nm laser pulse. No adjustments for the optical coupling of the laser into the reaction vessel or to the microwave lamp were made. With the known quantum yield for OH formation and cross section of HNO_3 at 248 nm, accurate measurement of the HNO_3 concentration and the laser fluence at 248 nm enabled us to calculate the OH concentration.

The smooth curves are the results of numerical simulations in which the initial concentrations of $(CH_3)_3N$ and NO_2 were used, as were the known rate constants for the reactions of $O(^3P)$ and OH with NO_2 (see above). The dotted lines are the predicted OH profile using the rate constant for OH + $(CH_3)_3N$ of 6.1×10^{-11} cm^3 s^{-1} as determined by ATK78/9. The solid lines use the present rate constant of 3.6×10^{-11} cm^3 s^{-1} for this reaction and clearly describe the OH decay much more accurately. For both of these sets of simulations, the lower curve is obtained by using a lower rate constant for $O(^3P) + (CH_3)_3N$ of 1.56×10^{-11} cm^3 s^{-1} as measured by Kirchner at al.[37] In addition to these rate constants, the branching ratio to OH formation was also varied to match approximately the observed OH concentration. Note that the variation of the branching ratio to OH has no effect other than to move the entire decay profile

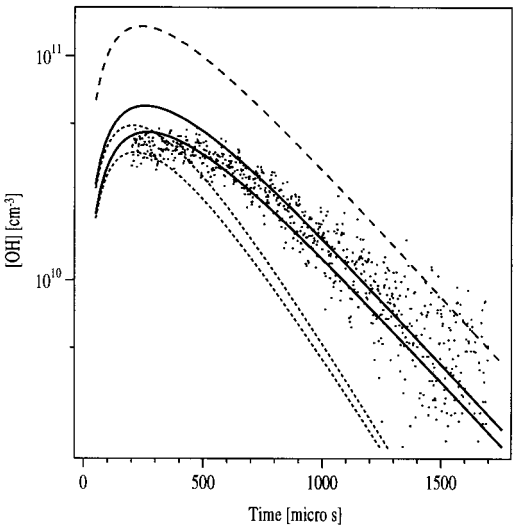

Figure 12. OH profiles following the 351 nm generation of $O(^3P)$ from NO_2 in the presence of $(CH_3)_3N$. For this experiment the initial conditions were $[(CH_3)_3N] = 0.66 \times 10^{14}$ cm^{-3}, $[NO_2] = 4.17 \times 10^{14}$ cm^{-3}, and $[O(^3P)] = 1.5 \times 10^{12}$ cm^{-3}. The smooth solid lines are the expected generation and decay of OH using $k_{OH+(CH_3)_3N} = 3.6 \times 10^{-11}$ cm^3 s^{-1}; the dotted lines were obtained by setting $k_{OH+(CH_3)_3N}$ to 6.1×10^{-11} cm^3 s^{-1}. For each of these pairs of curves, the upper one was obtained by using an $O(^3P) + (CH_3)_3N$ rate constant of 2.2×10^{-11} cm^3 s^{-1} and the lower one with 1.6×10^{-11} cm^3 s^{-1}. Both solid and dotted curves assume a branching ratio to OH formation of 30%. The dashed curve was obtained with a 100% branching ratio to OH formation and the slower reaction constants for both $O(^3P)$ and OH with $(CH_3)_3N$.

up or down. The same procedure was carried out with other data sets (not shown) in which the $(CH_3)_3N$ was varied. In all cases, the decay of OH at longer times [which is controlled by the rate of reaction with $(CH_3)_3N$] is well described by a rate constant close to 3.6×10^{-11} cm^3 s^{-1}. Although our data are not very sensitive to the rate of OH formation owing to the presence of laser-induced stray light that prevented measurement at $t < 150$ μs, we note that the lower rate constant for $O(^3P) + (CH_3)_3N$ of Kirchner et al.[37] more accurately describes our data. We therefore conclude that the ATK78/9 rate constant for $(CH_3)_3N$ is too high, and that for $O(^3P) + (CH_3)_3N$ might also be overestimated. Our data also provide an estimate of the yield of OH formation from the reaction of $O(^3P)$ with $(CH_3)_3N$ and is best matched with a branching ratio of $\approx$0.3. Considering errors in the calibration of our sensitivity to OH ($\pm$30%), errors in the determination of $(CH_3)_3N$ and NO_2 concentrations ($\pm$10%), and uncertainties in the rate constant for $O(^3P)$ with $(CH_3)_3N$, we estimate the branching ratio to be 0.30 ± 0.15.

In Table 1, we have summarized our results and compare them with the values obtained in the single previous study (ATK78/9). ATK78/9 used the resonance fluorescence technique to detect OH radicals generated by flash photolysis. With the exception of $(CH_3)_3N$ and CH_3NH_2, the results agree within the combined error uncertainties. For both CH_3NH_2 and $(CH_3)_3N$, our results are slightly lower than those of ATK78/9 but, as described above, the discrepancy cannot be explained by the re-formation of OH in reactions 17 or 20. To understand this discrepancy, we examine the major differences in the two experimental setups. The source of OH in the ATK78/9 experiments was the $\lambda \geq 105$ nm flash photolysis of H_2O vapor, and some of the photolysis light will also dissociate/excite the $(CH_3)_2NH$, which absorbs very strongly in the vacuum UV.[32] Experiments by ATK78/9 in which the flash energy was varied

suggest, however, that this did not measurably affect the OH kinetics.

ATK78/9 used substantially lower amine concentrations than in the present work with $0.25 \times 10^{13} < [CH_3NH_2] < 1.7 \times 10^{13}$, $0.5 \times 10^{12} < [(CH_3)_2NH] < 5.2 \times 10^{12}$, $0.25 \times 10^{13} < [C_2H_5NH_2] < 1.3 \times 10^{13}$ and $1.0 \times 10^{12} < [(CH_3)_3N] < 5.8 \times 10^{12}$ (units of cubic centimeters) and derived concentrations via partial flow and total pressure calculations. This method has disadvantages when dealing with "sticky" molecules, as the precise dilution of the amine in bath gas in a storage bulb is difficult. Our optical measurements of [amine] mean that our absolute mixing ratio of amine/Ar need not be known. The use of low concentrations in the ATK78/9 experiments also leads to the possibility that OH may react with other species in the Ar bath gas. The stated purity of Ar was >99.998% allowing a maximum impurity concentration of 3×10^{13} cm^{-3} at 50 Torr Ar and 298 K. If this impurity reacted only 1% as fast as the $(CH_3)_2NH$ with OH, this would increase the measured OH decay rates by a factor of 0.2.

Such effects are, however, too small to explain the ≈40% lower rate constant for $(CH_3)_3N$ and the 23% lower rate constant for CH_3NH_2. As our concentration measurements were based on direct UV absorption measurements and our absorption cross sections are in good agreement with those of Tannenbaum et al.,[32] we can identify no potential systematic error that might lower our rate constants by this amount. We have no rigorous explanation for the difference between these results and those of ATK78/9, but we point out that measurement of concentration directly by optical methods should yield a more reliable value than one based on calculated mixing ratios. Indeed, ATK78/9 draw attention to problems associated with a supplier's $(CH_3)_2NH$ mixing ratio, which those authors found to be erroneous by a factor of 1.9. We note further that the results of the same group for $O(^3P) + (CH_3)_3N$ and CH_3NH_2 are considerably higher that those of Kirchner et al.,[37] who measured rate constants that were some 30% and 60% lower for $(CH_3)_3N$ and CH_3NH_2, respectively, but in reasonable agreement for $C_2H_5NH_2$ and $(CH_3)_2NH$. This might indicate a mixing ratio error in the $(CH_3)_3N$ and CH_3NH_2 samples of ATK78/9.

As discussed by ATK78/9, the reactions of the OH radical with the amines above are thought to proceed via hydrogen atom abstraction from either a C−H or a N−H bond. The C−H bond is weaker than the N−H bond in CH_3NH_2 (and thus $C_2H_5NH_2$) by about 7 kcal/mol[38] and the H abstraction takes place mainly from a C−H bond, explaining the slight increase in OH reactivity of $C_2H_5NH_2$ compared to that of CH_3NH_2. For $(CH_3)_2NH$ the N−H bond is weaker and closer to the C−H bond energy. The greatly enhanced reactivity of $(CH_3)_2NH$ compared to CH_3NH_2 and $C_2H_5NH_2$ is thus mainly due to reaction at the N−H bond, and product studies have shown that about 37% of the reaction between OH and $(CH_3)_2NH$ proceeds via H abstraction from the N−H group.[9] The lack of an N−H bond in $(CH_3)_3N$ thus manifests itself as a lowering of the rate constant as compared to $(CH_3)_2NH$ but still more rapid than for CH_3NH_2 or $C_2H_5NH_2$ due to the increased number of C−H sites and the weaker C−H bond.[38]

Assuming a globally and diurnally averaged OH concentration of 1×10^6 OH cm^{-3}, our rate constant data yields lifetimes ($\tau_{1/2}$ in hours) of 16.3, 4.3, 7.7, and 9.9 for CH_3NH_2, $(CH_3)_2NH$, $(CH_3)_3N$, and $C_2H_5NH_2$, respectively.

5. Conclusions

We have remeasured the room-temperature kinetics of the OH reactions with four amines, CH_3NH_2, $(CH_3)_2NH$, $(CH_3)_3N$, and $C_2H_5NH_2$, using the two-photon dissociation of NO_2 in the presence of H_2 as a novel OH source. The results obtained for CH_3NH_2, $(CH_3)_2NH$, and $(CH_3)_3N$ are (in units of 10^{-11} cm^3 s^{-1}) 1.73 ± 0.11, 6.70 ± 0.47, and 3.58 ± 0.22, respectively. For $(CH_3)_2NH$ the results were confirmed using the 193 nm photolysis of N_2O in the presence of CH_4 as OH source [$k = (6.27 \pm 0.44) \times 10^{-11}$ cm^3 s^{-1}. The results for CH_3NH_2 and $(CH_3)_2NH$ are lower than the available literature data. For $C_2H_5NH_2$ [$k = (2.38^{+0.5}_{-0.15}) \times 10^{-11}$ cm^3 s^{-1}], our data are influenced by the regeneration of OH via reaction of the $O(^3P)$ byproduct of our of generation scheme with the amine. The present results highlight the potential use of two-photon dissociation of NO_2 in the presence of H_2 as a source of OH in pulsed photolysis kinetic studies when the "traditional" sources may be difficult to utilize but draw attention to potential shortcomings, especially related to the simultaneous formation of $O(^3P)$ and the competitive loss of OH due to reaction with NO_2.

References and Notes

(1) Finlayson-Pitts, B. J.; Pitts, J. N., Jr. *Atmospheric Chemistry* John Wiley and Sons: New York, 1986; Chapt. 4.

(2) Pilling, M. J.; Seakins, P. W. *Reaction Kinetics* Oxford University Press: New York, 1995; Chapt. 5.

(3) DeMore, W. B.; Sander, S. P.; Golden, D. M.; Hampson, R. F.; Kurylo, M. J.; Howard, C. J.; Ravishankara, A. R.; Kolb, C. E.; Molina, M. J. *Chemical Kinetics and Photochemical Data for Use in Stratospheric Modeling*; JPL Publication 97-4: Pasadena, CA, 1997.

(4) Carl, S. A.; Horowitz, A.; Wollenhaupt, M.; Crowley, J. N. Rate constants for reaction of OH with C_3H_8 (298 K), *i*-C_3H_7I (298 K), *n*-C_3H_7I (298 K), and $CH_3C(O)CH_3$ (221−395 K). To be submitted for publication, 1998.

(5) Schade, G. W.; Crutzen, P. J. *J. Atmos. Chem.* **1995**, *22*, 319 (and references therein).

(6) Intergovernmental Panel on Climatic Change (IPCC). *Climate Change*; The supplementary report to the IPCC Scientific Assessment; Houghton, J. T., Rasmussen, Callander, B. A., Varnay, S. K., Eds.; Cambridge University Press: New York, 1992.

(7) Crutzen, P. J. *J. Geophys. Res.* **1971**, *76*, 7311.

(8) McElroy, M. B.; McConnell, J. C. *J. Atmos. Sci.* **1971**, *28*, 1095.

(9) Lindley, C. R. C.; Calvert, J. G.; Shaw, J. H. *Chem. Phys. Lett.* **1979**, *67*, 57.

(10) Atkinson, R.; Perry, R. A.; Pitts, J. N., Jr. *J. Chem. Phys.* **1977**, *66*, 1578.

(11) Atkinson, R.; Perry, R. A.; Pitts, J. N., Jr. *J. Chem. Phys.* **1978**, *68*, 1850.

(12) Crowley, J. N.; Campuzano-Jost, P.; Moortgat, G. K. *J. Phys. Chem.* **1996**, *100*, 3601.

(13) Crowley, J. N.; Carl, S. A. *J. Phys. Chem.* **1997**, *101*, 4178.

(14) Schneider, W.; Moortgat, G. K.; Tyndall, G. S.; Burrows, J. P. *J. Photochem. Photobiol. A* **1987**, *40*, 195.

(15) Uselman, W. A.; Lee, E. K. C. *J. Chem. Phys.* **1976**, *65*, 1948.

(16) Shi, J.; Barker, J. R. *Int. J. Chem. Kinetics* **1990**, *22*, 1283 (and references therein).

(17) Donahue, N. M.; Dubey, M. K.; Mohrschladt, R.; Demerjian, K. L.; Anderson, J. G. *J. Geophys. Res.* **1998**, *102*, 6159 (and references therein).

(18) Sloan, J. J. *J. Phys. Chem.* **1988**, *92*, 18.

(19) Silver, J. A.; Dimpfl, W. L.; Brophy, J. H.; Kinsey, J. L. *J. Chem. Phys.* **1976**, *65*, 1811.

(20) Rensberger, K. J.; Jeffries, J. B.; Crosley, D. R. *J. Chem. Phys.* **1989**, *90*, 2174.

(21) Smith, I. W. M.; Williams, M. D. *J. Chem. Soc., Faraday Trans. 2* **1985**, *81*, 1849.

(22) Carl, S. A.; Crowley, J. N. Unpublished data.

(23) Anderson, J. G.; Margitan, J. J.; Kaufman, F. *J. Chem. Phys.* **1974**, *60*, 3310.

(24) Howard, C. J.; Evenson, K. M. *J. Chem. Phys.* **1974**, *61*, 1943.

(25) Erler, K.; Field, D.; Zellner, R.; Smith, I. W. M. *Ber. Bunsen-Ges. Phys. Chem.* **1977**, *81*, 22.

(26) Anderson, L. G. *J. Phys. Chem.* **1980**, *84*, 2152.

(27) Burrows, J. P.; Wallington, T. J.; Wayne, R. P. *J. Chem. Soc., Faraday Trans.* **1983**, *79*, 111.

(28) Hanst, P. L.; Spence, J. W.; Miller, M. *Environ. Sci. Technol.* **1977**, *11*, 403.

(29) Pitts, J. N., Jr.; Grosjean, D.; Van Cauwenberghe, K.; Schmid, J. P.; Fitz, D. R. *Environ. Sci. Technol.* **1978**, *12*, 946.
(30) Waschewsky, G. C. G.; Kitchen, D. C.; Browning, P. W.; Butler, L. J. *J. Phys. Chem.* **1995**, *99*, 2635.
(31) Haak, H. K.; Stuhl, F. *J. Phys. Chem.* **1984**, *88*, 3627.
(32) Tannenbaum, E.; Coffin, E. M.; Harrison, A. J. *J. Chem. Phys.* **1953**, *21*, 311.
(33) Okabe, H. *The photochemistry of small molecules*; John Wiley and Sons: New York, 1989.
(34) Biggs, P.; Canosa-Mas, C. E.; Fracheboud, J.-M.; Parr, A. D.; Shallcross, D. E.; Wayne, R. P.; Caralp, F. *J. Chem. Soc., Faraday Trans.* **1993**, *89*, 4163.
(35) Atkinson, R.; Pitts, J. N., Jr. *J. Chem. Phys.* **1978**, *68*, 911.
(36) Curtis, A. R.; Sweetenham, W. P. *Facsimile program*; AERE Report R-12805; Her Majesty's Stationery Office: London, 1987.
(37) (a) Kirchner, K.; Merget, N.; Schmidt, C. *Chem. Ing. Technol.* **1974**, *46*, 661. (b) Kirchner, K. *Int. J. Chem. Kinetics* **1975**, *1*, 103.
(38) Atkinson, R. *Chem. Rev.* **1986**, *86*, 69.